JACS
JOURNAL OF THE AMERICAN CHEMICAL SOCIETY

Article

pubs.acs.org/JACS

Exposing the Flexibility of Human Parainfluenza Virus Hemagglutinin-neuraminidase

Moritz Winger* and Mark von Itzstein*

Institute for Glycomics, Gold Coast Campus, Griffith University Queensland, 4222, Australia

Supporting Information

ABSTRACT: Human parainfluenza virus type 3 (hPIV-3) is a clinically significant pathogen and is the causative agent of pneumonia and bronchiolitis in children. In this study the solution dynamics of human parainfluenza type 3 hemagglutinin-neuraminidase (HN) have been investigated. A flexible loop around Asp216 that adopts an open conformation in direct vicinity of the active site of the *apo*-form of the protein and closes upon inhibitor binding has been identified. To date, no available X-ray crystal structure has shown the molecular dynamics simulation-derived predominant loop-conformation states found in the present study. The outcomes of this study provide additional insight into the dynamical properties of hPIV-3 HN and may have important implications in defining HN glycan recognition events, receptor specificity, and antiparainfluenza virus drug discovery.

INTRODUCTION

Viruses are one of the greatest health threats[1] to mankind, and viral diseases have significant socioeconomic impact on the world.[2] The *Paramyxoviridae* family of viruses is of significant medical and veterinary importance,[3] including the important human respiratory pathogens, the parainfluenza viruses (hPIVs). hPIV types 1 to 3 are the leading cause of respiratory disease in infants and young children, the immunocompromised, chronically ill, and elderly.[3,4] Clinical manifestation of parainfluenza infection is typically croup[5] (hPIV-1) and pneumonia or bronchiolitis (hPIV-3).[6] Up to 100 000 hospitalizations per annum in the USA alone occur as a result of parainfluenza virus infection. Despite a number of attempts, there are currently neither vaccines[7] nor specific antiviral therapy[8] to prevent or treat hPIV infections. While hPIV vaccine development continues,[9] there is an urgent need for the discovery of specific cost-effective antiparainfluenza drugs.

Paramyxoviral hemagglutinin-neuramindase (HN) is a glycoprotein associated with the outer membrane of the virus particle and is essential for the initial glycan-mediated binding of the virus to the host cell as well as for the release of virus progeny from the infected host cell.[3] The crystal structures of the paramyxoviral HN show that the architecture of the active site is similar to influenza virus sialidase (NA)[10,11] with six of seven[12] critical active site amino acids functionally conserved.[10,11,13]

The *N*-acetylneuraminic acid-based sialidase inhibitor Neu5Ac2en (**1**)[14−17] and the potent influenza virus sialidase inhibitor 4-deoxy-4-guanidino-Neu5Ac2en (zanamivir, **2**)[14,16−18] have been evaluated against the hPIVs 1 to 3 sialidase activity in various in vitro assays, with inhibition values reported in the high micromolar range. Significantly, both Neu5Ac2en (**1**)[19] and zanamivir (**2**)[17,20] have also been shown to inhibit the receptor-binding and fusion processes of hPIV-3. In comparison to intensive research into influenza virus sialidase inhibitor development,[1,21] there have been relatively few studies reported on the development of inhibitors of hPIV HN sialidase activity. Glycan array studies[22,23] have provided insight into the receptor specificity of hPIV HN as well as an exploration of a secondary carbohydrate-binding site. Moreover, a C4−C5 difuncitonalized Neu5Ac2en derivative that contains more bulky substituents than either **1** or **2** can also be accommodated within the hPIV HN active site.[22]

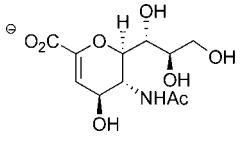

1

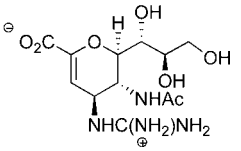

2

In recent molecular dynamics (MD) studies on influenza A virus sialidase, loop flexibility in two distinct regions (the 150-loop and the 430-loop) that are in close proximity to the protein's active site has been observed.[24,25]

Our present study on hPIV-3 HN uses Molecular Dynamics (MD) simulations on four different hPIV-3 HN structures to investigate the structural dynamics of this protein in solution. Specifically, to explore hPIV HN loop flexibility, we have investigated two *apo*-forms of the enzyme crystallized at the two different pH values 6.5 and 7.5 (PDB 1V2I, 1V3B), one structure in complex with Neu5Ac2en (**1**, PDB 1V3D), and one in complex with zanamivir (**2**, PDB 1V3E).[10] Complexed

Received: August 29, 2012
Published: October 11, 2012

   dx.doi.org/10.1021/ja3084658 | *J. Am. Chem. Soc.* 2012, 134, 18447−18452

structures have been crystallized at pH 7.5. The outcomes of this study will have significant implications in the discovery of novel antiparainfluenza inhibitors.

METHODS

Molecular Dynamics Simulations. MD simulations were performed with the GROMOS software[26,27] using the force-field parameter set 54A4.[28] Initial coordinates were taken from the X-ray structure of hPIV-3 HN[10] (PDB: 1V2I, 1V3B), in complex with 2-deoxy-2,3-didehydro-D-*N*-acetylneuraminic acid (Neu5Ac2en, **1**)[10] (PDB: 1V3D) and in complex with zanamivir (**2**)[10] (PDB: 1V3E). In Figure 1, a superimposition of all available crystal structures shows

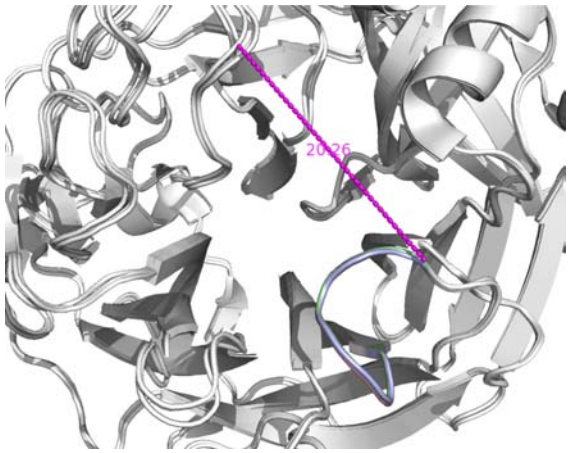

Figure 1. Superimposition of the experimental crystal structures of hPIV-3 NA (1V2I, 1V3B, 1V3D, 1V3E[10]). The distance across the cavity size is 20.26 Å.

that the structures solved for both *apo*- and *holo*-forms of hPIV-3 HN exhibit closed-loop conformations for the 216-loop. Parameters for **1** and **2** have been generated (Supporting Information) in an analogous manner to existing parameters in the GROMOS force-field. Ionization states of amino acid residues were assigned at pH 7.0. The histidine side chains were protonated at the N_ε atom. Calcium and sulfate ions present in the crystal structure have been included in the simulation. The simple-point-charge (SPC) water model[29] was used to describe the solvent molecules. In the simulations, water molecules were added around the protein within a cubic box with a minimum distance of 1.4 nm between the protein atoms and the square walls of the periodic box. All bonds were constrained with a geometric tolerance of 10^{-4} using the SHAKE algorithm.[30]

A steepest-descent energy minimization of the system was performed to relax the solute−solvent contacts while positionally restraining the solute atoms using a harmonic interaction with a force constant of 2.5×10^4 kJ mol^{-1} nm^{-2}. Next, steepest-descent energy minimization of the system without any restraints was performed to eliminate any residual strain. The energy minimizations were terminated when the energy change per step became smaller than 0.1 kJ mol^{-1}. For the nonbonded interactions, a triple-range method with cutoff radii of 0.8/1.4 nm was used. Short-range van der Waals and electrostatic interactions were evaluated every time step based on a charge-group pair list. Medium-range van der Waals and electrostatic interactions, between (charge group) pairs at a distance longer than 0.8 nm and shorter than 1.4 nm, were evaluated every fifth time step, at which point the pair list was updated. Outside the longer cutoff radius, a reaction-field approximation[31] was used with a relative dielectric permittivity of 78.5. The center of mass motion of the whole system was removed every 1000 time steps. Solvent and solute were independently, weakly coupled to a temperature bath of 295 K with a relaxation time of 0.1 ps.[32]

The systems were also weakly coupled to a pressure bath of 1 atm with a relaxation time of 0.5 ps and an isothermal compressibility of 0.7513×10^{-3} (kJ mol^{-1} nm^{-3})$^{-1}$. Periods of 20 ps MD simulation with harmonic position restraining of the solute atoms with force constants of 2.5×10^4, 2.5×10^3, 2.5×10^2, and 2.5×10^1 kJ mol^{-1} nm^{-2} were performed to further equilibrate the systems at 50, 120, 1800, 240, and 300 K, respectively. The simulations were each carried out for 30 ns. The trajectory coordinates and energies were saved every 0.5 ps for analysis. Performed simulations are summarized in Table 1.

Analysis. Analyses were done with the analysis software GROMOS ++.[33] Atom-positional root-mean-square differences (RMSDs) between structures were calculated by performing a rotational and translational atom-positional least-squares fit of one structure on the second (reference) structure using a given set of atoms (N, C_α, C).

Atom-positional root-mean-square fluctuations (RMSFs) over a period of simulation were calculated by performing a rotational and translational atom-positional least-squares fit of the C_α-atoms of the trajectory structures on the reference. RMSFs have been calculated for all residues and for the residues comprising the 216-loop (residues 210−221). To obtain reduced, representative structural ensembles for the simulations, RMSD-based conformational clustering has been performed.[34] Structures extracted every 10 ps from simulations have been superimposed on backbone-C_α atoms to remove overall rotation and translation. Clustering of the residues that line the binding site (residues 190−198, 210−221, 251−259, 274−280, 320−326, 334−339, 369−377, 407−413, 474−480, 529−533) has been performed to compare relative structural populations of hPIV-3 HN protein from the different simulation trajectories. The similarity criterion applied in this analysis was the RMSD of all residue atoms with a cutoff of 0.13 nm, as previously described[24] for influenza virus sialidase. The percentages of intermolecular hydrogen (H) bonds between the protein and ligand have been calculated for the simulations involving Neu5Ac2en- (**1**) and zanamivir- (**2**) bound structures (1V3D, 1V3E) using a maximum distance criterion of 0.25 nm between the hydrogen atom and the acceptor atom and a minimum donor−hydrogen−acceptor angle criterion of 135°.

RESULTS

The simulations of the four available crystal structures allow an investigation of the different dynamic behavior of hPIV-3 HN in solution and under physiological conditions. The atom-positional root-mean-square deviations (RMSDs) from the starting structures for the atoms (C_α, N, C) in the simulations are shown in Figure 2. All of the proteins studied remain close to their starting crystal structures, and their RMSDs converge to a value of approximately 0.2 nm (Figure 2, Panel A). The overall backbone RMSD shows that all of the simulated systems remain stable during the 30 ns of production. The RMSD

Table 1. Overview of the MD Simulations of the Different Systems[a]

simulation label	1V2I	1V3B	1V3D	1V3E
protein	*apo*-hPIV-3 HN	*apo*-hPIV-3 HN	hPIV-3 HN−(**1**) complex	hPIV-3 HN−(**2**) complex
starting structure (PDB ID)	1V2I	1V3B	1V3D	1V3E
simulation length [ns]	30	30	30	30

[a]1V2I: *apo*-hPIV-3 HN;[10] 1V3B: *apo*-hPIV-3 HN;[10] 1V3D: hPIV-3 in complex with Neu5Ac2en (**1**);[10] 1V3E: hPIV-3 HN in complex with zanamivir (**2**).[10]

dx.doi.org/10.1021/ja3084658 | J. Am. Chem. Soc. 2012, 134, 18447−18452

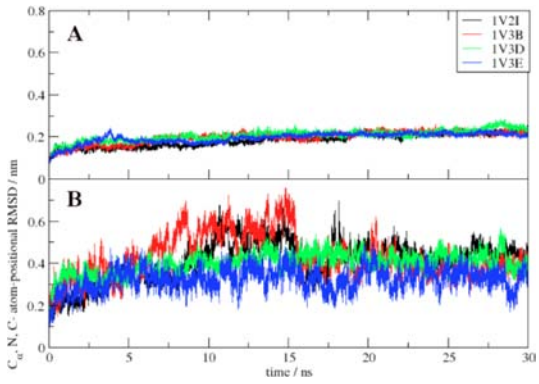

Figure 2. Atom-positional RMSDs of the backbone atoms (C_α, N, C). 1V2I (black), 1V3B (red), and 1V3D in complex with Neu5Ac2en (**1**, green) and 1V3E with zanamivir (**2**, blue), with respect to the starting (X-ray) structure in the simulations. RMSDs have been calculated for all residues (Panel A) and the 216-loop (residues 210−221, B). The protein's overall structure remains close to the crystal structure; conformational rearrangements, however, are observed for the 216-loop in the *apo*-protein (Panel B, black and red curves).

values calculated for residues comprising the 216-loop region (residues 210−221) (Figure 2, Panel B) reach plateau values of around 0.3 nm for all simulations, except for 1V2I and 1V3B, where elevated RMSD values of around 0.6 nm are reached for a period of 5 ns during the simulation. Deviation from the crystal starting structure seems to be more significant in these simulations, indicating a loop-opening transition and supporting the notion that complexation of Neu5Ac2en (**1**) and zanamivir (**2**) stabilizes a closed-loop conformation of the hPIV-3 HN protein.

The atom-positional root-mean-square fluctuations (RMSFs) for the C_α-atoms were calculated for the entire 30 ns of the trajectories (Figure 3). All simulations show reasonably small fluctuations for secondary structure regions, indicating that secondary structure features of all systems remain intact. Larger fluctuations are observed for the loop regions. Fluctuations for the 216-loop (residues 210−221) vary in the different simulations (Figure 4), reaching values of up to 0.3 nm for

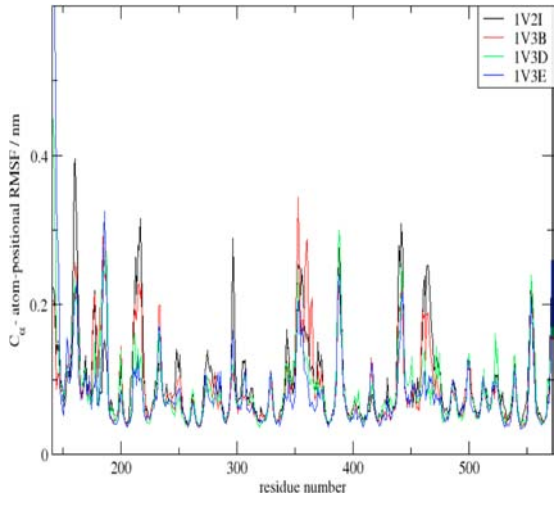

Figure 3. Atom-positional RMSFs of the C_α atoms. 1V2I (black), 1V3B (red), and 1V3D in complex with Neu5Ac2en (**1**, green) and 1V3E with zanamivir (**2**, blue) over the entire simulation time. The least-squares superimposition of structures involved all C_α atoms.

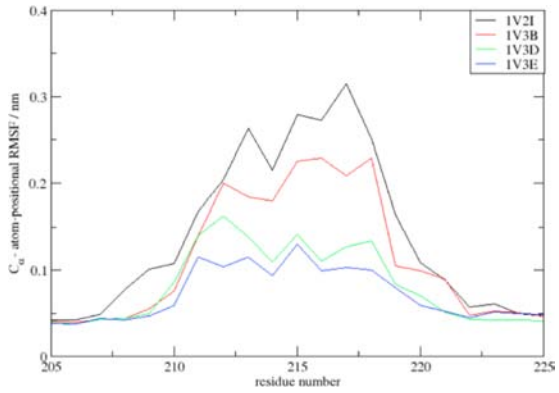

Figure 4. Atom-positional RMSFs of the C_α atoms comprising the 216-loop. 1V2I (black), 1V3B (red), and 1V3D in complex with Neu5Ac2en (**1**, green) and 1V3E with zanamivir (**2**, blue) over the entire simulation time. The least-squares superposition of structures involved all C_α atoms. The 216-loop of inhibitor-bound structures showed lower fluctuations than the *apo*-forms of the protein.

the simulations of the *apo*-structures 1V2I and 1V3B, indicating that this region of the protein is highly flexible in the *apo*-forms of the protein.

Simulations of the hPIV-3 HN−ligand complexes exhibit smaller RMSF values of around 0.1 nm, emphasizing the stabilizing effect ligand binding has on the 216-loop's conformation. Binding of zanamivir (**2**) leads to smaller fluctuations than Neu5Ac2en (**1**), suggesting a higher inhibition efficacy of zanamivir (**2**) in comparison to Neu5Ac2en (**1**). RMSF values of a selection of hot-spot residues lining the catalytic site are presented (Table 2).

Table 2. Root-Mean-Square Fluctuations of Selected Residues Comprised in the 216-Loop for the Simulated Systems in Nanometers

residue	X-ray	1V2I	1V3B	1V3D	1V3E
210	0.036	0.108	0.076	0.086	0.059
212	0.046	0.204	0.200	0.163	0.104
214	0.048	0.215	0.179	0.109	0.093
216	0.057	0.273	0.229	0.111	0.099
218	0.060	0.252	0.229	0.134	0.100
220	0.041	0.109	0.099	0.070	0.059

The dynamics of these residues are of particular interest for structure-based inhibitor design investigations. This analysis reveals elevated RMSF values in the immediate surroundings of residue Asp216 for the simulation of 1V2I and 1V3B in comparison to the simulations with bound ligands (**1**) 1V3D (**2**) and 1V3E. The zanamivir (**2**)-bound structure undergoes the least amount of movement away from the starting crystal structure. Comparison of the RMSF values obtained from the simulation of the *apo*-structures to values obtained from experimental *B*-values shows that in the crystal structure the 216-loop is significantly more rigid than in solution. The most populated clusters of all simulations are shown (Figure 5) in comparison with the experimentally derived crystal structure of hPIV-3 HN.[10]

These results suggest that significant motion can occur in the 216-loop, and it is highly governed by the absence or presence of a ligand. The *apo*-systems seem to be more flexible in the catalytic region, compared to the systems where either **1** or **2** is

dx.doi.org/10.1021/ja3084658 | J. Am. Chem. Soc. 2012, 134, 18447−18452

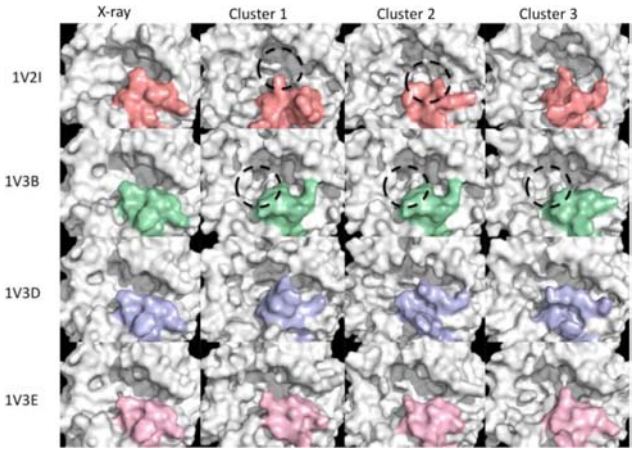

Figure 5. Three most populated clusters (second, third, and fourth column) of the 216-loop in the simulations of the *apo*-structures 1V2I (first row) and 1V3B (second row), as well as for the ligand-bound structures 1V3D with Neu5Ac2en (**1**, third row) and 1V3E with zanamivir (**2**, fourth row). Shown in comparison is the experimental crystal structures[10] (first column). Solvent-accessible surface plots of the active site's cavity are shown. Significant changes in the conformation of the 216-loop are indicated by dashed circles. The 216-loop is shown in color (residue 210−221).

bound. The solvent-accessible surface of the three most populated cluster conformations occurring in the simulations is also shown (Figure 5). The simulations of the *apo*-structures present a larger, more accessible cavity than the simulations with bound substrate as is indicated by dotted circles (Figure 5).

To further describe the nature of the open-loop conformation, Figure 6 shows the superimposition of the crystal structure of *apo*-hPIV-3 HN (1V2I[10]) with the most populated structural cluster obtained from a MD simulation of the same structure. The distance between the cavity walls shows an increased value for the MD simulation.

Final conformations (Figure 7) of the 216-loop after 10 and 20 ns of simulations have been determined. We observed that

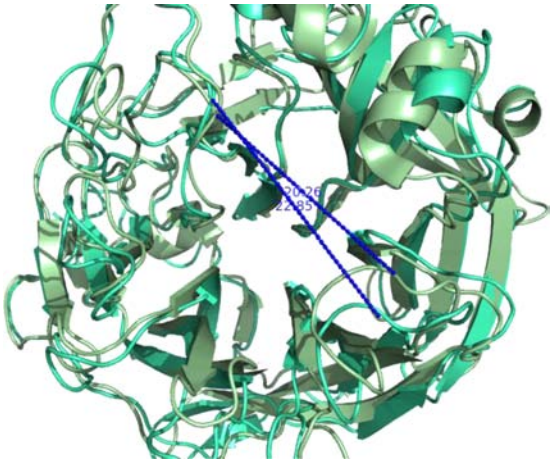

Figure 6. Superimposition of the crystal structure of hPIV-3 HN (1V2I,[10] dark green) and the most populated cluster of the corresponding MD simulation (light green). The distances between the walls of the binding site are labeled in blue, 20.26 and 22.85 Å for the structurally observed and MD calculated, more open structure, respectively.

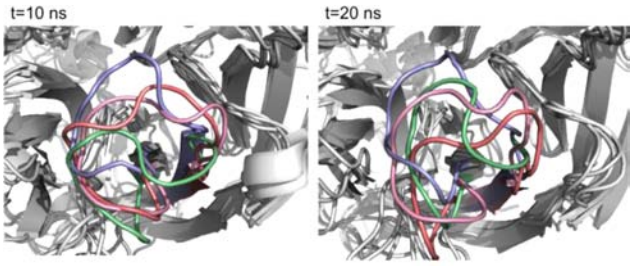

Figure 7. Superimposed final structures after 10 ns (left) and 20 ns (right) of the simulations 1V2I (*apo*, red), 1V3B (*apo*, green), 1V3D (Neu5Ac2en, **1**, blue), and 1V3E (zanamivir, **2**, magenta). Open-loop conformations are preferred for the *apo*-forms of hPIV-3 HN, whereas the ligand-bound structures adopt closed-loop conformations.

the simulations of the *apo*-forms 1V2I and 1V3B undergo conformational changes. In the simulation of 1V3B, the loop adopts a fully opened conformation after 10 ns, whereas the ligand-bound structures show closed-loop conformations at all stages of the simulations.

The hydrogen bond interactions between the C4-hydroxyl group of **1** and the Asp216 side chain, that further stabilize the closed-loop conformation, have been determined (Figure 8 and Table 3). Interestingly, in the simulation of hPIV-3 HN with **2**, however, no such interaction was observed (Figure 8).

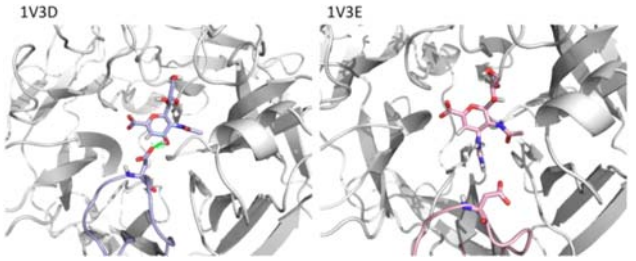

Figure 8. Final structures of the hPIV-3 HN bound to the inhibitors Neu5Ac2en (**1**, left) and zanamivir (**2**, right). The residue Asp216 is explicitly shown. A persistent hydrogen bond between Neu5Ac2en (**1**) and Asp216 further stabilizes the closed-loop conformation (green line). This hydrogen bond engagement is not observed in the case of zanamivir (**2**) bound within the active site.

Table 3. Occurrence (%) of Hydrogen (H) Bonds Involving Asp216 from the 30 ns MD Simulation of 1V3D[a]

donor molecule	donor atom	acceptor residue	acceptor atom (O)	H-bond %
Neu5Ac2en	C4-OH	Asp216	O1	29
Neu5Ac2en	C4-OH	Asp216	O2	58

[a]Zanamivir (**2**) (simulation 1V3E) did not show significant hydrogen bonding with Asp216 in the course of the 30 ns of simulations.

DISCUSSION

We have used a Molecular Dynamics (MD) simulation approach to identify a flexible region of the hPIV-3 HN protein that lies in immediate vicinity to the *N*-acetylneuraminic acid binding site. hPIV-3 HN is an essential protein in the lifecycle of the virus and is used by the virus in both attachment and release from host cells. Our study represents the first MD investigation on a validated drug discovery target for antiparainfluenza virus therapeutics development. The loop comprising the residues 210−221, the so-called 216-loop,

dx.doi.org/10.1021/ja3084658 | J. Am. Chem. Soc. 2012, 134, 18447−18452

populates different conformations in the *apo*-form of the HN in comparison to the inhibitor-bound protein.

Our data suggest that the 216-loop is in a more open conformation in the *apo*-protein, and when either substrate or inhibitor is bound the loop closes to better engage the ligand. Interestingly, all of the available experimentally determined structures[10] do not show differences in the 216-loop conformation between inhibitor-bound structures and *apo*-structures. All of these experimentally determined structures have a closed-loop conformation, and this fact is reminiscent of the experimentally derived influenza A virus Group 2 sialidase structures.[1] The present study, however, demonstrates that the 216-loop cannot be treated as a rigid, defined characteristic for the hPIV HN protein. We conclude that the 216-loop can adopt an open conformation in solution under physiological conditions (pH 7, 298 K, 1 atm). This phenomenon is consistent with recently published findings[22,23] which showed that larger ligands can be accommodated in hPIV-3 NA's binding site. It is likely that flexibility plays an important role in ligand binding, particularly glycan-receptor recognition, and mechanism of catalysis studies for hPIV-3 HN should take into account the different conformations that the 216-loop can adopt. A similar phenomenon has been observed for influenza A virus group 1 (e.g., N1) and group 2 (e.g., N2) sialidases, where some crystal structures of both groups have been obtained exclusively in closed-loop conformations. However, recent results of MD studies suggest that loop flexibility exists across both groups, and this observation has become a subject of interest for further influenza A virus sialidase inhibitor development.[24,25]

CONCLUSION

These recent MD investigations,[24,25] taken together with our present study, lead us to propose that this loop flexibility may be a common feature of all viral sialidases and may be an important determinant of glycan receptor specificity. The current study further highlights the importance of dynamic simulations in better understanding potential protein flexibility that has not been resolved by crystallographic analysis. Our present findings provide new opportunities toward a better understanding of glycan (receptor) recognition and the discovery of novel therapeutics to treat parainfluenza viral infections. Finally, this study further supports the notion that protein flexibility may be a common feature of glycan-binding proteins, particularly glycan-recognizing enzymes.

ASSOCIATED CONTENT

Supporting Information

Parameters for the MD simulations are provided. This material is available free of charge via the Internet at http://pubs.acs.org.

AUTHOR INFORMATION

Corresponding Author

m.winger@griffith.edu.au; m.vonitzstein@griffith.edu.au

Notes

The authors declare no competing financial interest.

ACKNOWLEDGMENTS

This manuscript is dedicated to Professor Wilfred F. van Gunsteren, and the authors would like to acknowledge Jeffrey C. Dyason. The authors gratefully acknowledge the Australian Research Council for financial support and access to the Griffith University Gowonda HPC Cluster.

REFERENCES

(1) von Itzstein, M.; Thomson, R. *Handb. Explor. Pharmacol.* **2009**, *189*, 111.
(2) Fendrick, A. M.; Monto, S. A. *Arch. Intern. Med.* **2003**, *163*, 487.
(3) Henrickson, K. J. *Clin. Microbiol. Rev.* **2003**, *16*, 242.
(4) Nichols, W. G.; Peck Campbell, A. J.; Boeckh, M. *Clin. Microbiol. Rev.* **2008**, *21*, 274.
(5) Reed, G.; Jewett, P. H.; Thompson, J.; Tollefson, S.; Wright, P. F. *J. Infect. Dis.* **1997**, *175*, 807.
(6) Heilman, C. A. *J. Infect. Dis.* **1990**, *161*, 402.
(7) Schmidt, A. C.; Schaap-Nutt, A.; Bartlett, E. J.; Schomacker, H.; Boonyaratanakornkit, J.; Karron, R. A.; Collins, P. L. *Expert Rev. Respir. Med.* **2011**, *5*, 515.
(8) DeLaMora, P.; Moscona, A. *Pediatr. Transplant.* **2007**, *11*, 121.
(9) Karron, R. A.; Thumar, B.; Schappell, E.; Surman, S.; Murphy, B. R. P.; Collins, L.; Schmidt, A. C. *Vaccine* **2012**, *30*, 3975.
(10) Lawrence, M. C. *J. Mol. Biol.* **2004**, *335*, 1343.
(11) Crennell, S.; Takimoto, T.; Portner, A.; Taylor, G. *Nat. Struct. Biol.* **2000**, *7* (11), 1068.
(12) Yuan, P.; Thompson, T. B.; Wurzburg, B. A.; Paterson, R. G.; Lamb, R. A.; Jardetzky, T. S. *Structure* **2005**, *13*, 803.
(13) Langendijk, J. P. M. *J. Virol.* **1997**, *71*, 6155.
(14) Tindal, D. J.; Dyason, J. C.; Thomson, R. J.; Suzuki, T.; Ueyama, H.; Kuwahara, Y.; Maki, N.; Suzuki, Y.; von Itzstein, M. *Bioorg. Med. Chem. Lett.* **2007**, *17* (6), 1655.
(15) Suzuki, T.; Ikeda, K.; Koyama, N.; Hosokawa, C.; Kogure, T.; Takahashi, T.; Jwa Hidari, K. I.; Miyamoto, D.; Tanaka, K.; Suzuki, Y. *Glycoconjugate J.* **2001**, *18* (4), 331.
(16) Holzer, C. T.; von Itzstein, M.; Jin, B.; Pegg, M. S.; Stewart, W. P.; Wu, W. Y. *Glycoconjugate J.* **1993**, *10* (1), 40.
(17) Greengard, O.; Poltoratskaia, N. L., E.; Zimmerberg, J.; Moscona, A. *J. Virol.* **2000**, *74*, 11108.
(18) von Itzstein, M.; Wu, W. Y.; Kok, G. B.; Pegg, M. S.; Dyason, J. C.; Jin, B.; Van Phan, T.; Smythe, M. L. a. W., H. F.; Oliver, S. W.; Colman, P. M.; Varghese, J. N.; Ryan, D. M.; Woods, J. M.; Bethell, R. C.; Hotham, V. J.; Cameron, J. M.; Penn, C. R. *Nature* **1993**, *363*, 418.
(19) Levin Perlman, S.; Jordan, M.; Brossmer, R.; Greengard, O.; Moscona, A. *Virology* **1999**, *265* (1), 57.
(20) Porotto, M.; Greengard, O.; Poltoratskaia, N.; Horga, M. A.; Moscona, A. *J. Virol.* **2001**, *75* (16), 7481.
(21) von Itzstein, M. *Nat. Rev. Drug Discovery* **2007**, *6*, 967.
(22) Alymova, I. V.; Portner, A.; Mishin, V. P.; McCullers, J. A.; Freiden, P.; Taylor, G. L. *Glycobiology* **2012**, *22*, 174.
(23) Amonsen, M.; Smith, D. F.; Cummings, R. D.; Air, G. M. *J. Virol.* **2007**, *81*, 8341.
(24) Amaro, R. E.; Cheng, X.; Ivanov, I.; Xu, D.; McCammon, J. A. *J. Am. Chem. Soc.* **2009**, *131*, 4702.
(25) Amaro, R. E.; Swift, R. V.; Votapka, L.; W., L. W.; Walker, R. C.; Bush, R. M. *Nat. Commun.* **2011**, *2:388*, 1.
(26) van Gunsteren, W. F.; Billeter, S. R.; Eising, A. A.; Hünenberger, P. H.; Krüger, P.; Mark, A. E.; Scott, W. R. P.; Tironi, I. G. *Biomolecular Simulation: The GROMOS Manual and User Guide*; vdf Hochschulverlag, ETH Zürich: Switzerland, 1996.
(27) Scott, W. R. P.; Hünenberger, P. H.; Tironi, I. G.; Mark, A. E.; Billeter, S. R.; Fennen, J.; Torda, A. E.; Huber, T.; Krüger, P.; van Gunsteren, W. F. *J. Phys. Chem. A* **1999**, *103*, 3596.
(28) Schmid, N.; Eichenberger, A.; Choutko, A.; Riniker, S.; Winger, M.; Mark, A. E.; van Gunsteren, W. F. *Eur. Biophys. J.* **2011**, *40*, 843.
(29) Berendsen, H. J. C.; Postma, J. P. M.; van Gunsteren, W. F.; Hermans, J. In *Intermolecular forces*; Pullman, B., Ed.; Reidel: Dordrecht, 1981; p 331.
(30) Ryckaert, J.-P.; Ciccotti, G.; Berendsen, H. J. C. *J. Comput. Phys.* **1977**, *23*, 327.
(31) Tironi, I. G.; Sperb, R.; Smith, P. E.; van Gunsteren, W. F. *J. Chem. Phys.* **1995**, *102*, 5451.

(32) Berendsen, H. J. C.; Postma, J. P. M.; van Gunsteren, W. F.; Di Nola, A.; Haak, J. R. *J. Chem. Phys.* **1984**, *81*, 3684.
(33) Christen, M.; Hünenberger, P. H.; Bakowies, D.; Baron, R.; Bürgi, R.; Geerke, D. P.; Heinz, T. N.; Kastenholz, M. A.; Kräutler, V.; Oostenbrink, C.; Peter, C.; Trzesniak, D.; van Gunsteren, W. F. *J. Comput. Chem.* **2005**, *26*, 1719.
(34) Daura, X.; Jaun, B.; Seebach, D.; van Gunsteren, W. F.; Mark, A. E. *J. Mol. Biol.* **1998**, *280*, 925.